ISTITUTO NAZIONALE DI FISICA NUCLEARE

Sezione di Milano

INFN/BE-96/09
27 Novembre 1996

P. Guazzoni, M. Jaskola, L. Zetta, J. Gu, A. Vitturi
G. Graw, R. Hertenberger, D. Hofer, P. Schiemenz, B. Valnion, E. Zanotti-Müller
U. Atzrott, G. Staudt

STUDY OF THE $^{90}Zr(\vec{p},\alpha)^{87}Y$ REACTION AT 22 MeV

Poster Contribution to EPS10
Trends in Physics Conference, September 9,14, 1996 Sevilla

SIS - Pubblicazioni
dei Laboratori Nazionali di Frascati

INFN – Istituto Nazionale di Fisica Nucelare
Sezione di Milano

INFN/BE–96/09
27 Novembre 1996

STUDY OF THE $^{90}Zr(\vec{p},\alpha)^{87}Y$ REACTION AT 22 MeV

P. Guazzoni, M. Jaskola[†] and L. Zetta
Dipartimento di Fisica dell'Università and I.N.F.N. via Celoria 16, I-20133 Milano, Italy

J. Gu [‡] and A. Vitturi
Dipartimento di Fisica dell'Università and I.N.F.N. via Marzolo 8, I-35100 Padova, Italy

G. Graw, R. Hertenberger, D. Hofer, P. Schiemenz, B. Valnion and E. Zanotti-Müller
Sektion Physik der Universität München, D-85748 Garching, Germany

U. Atzrott and G. Staudt
Physikalisches Institut der Universität, Auf der Morgenstelle 14, D-72076 Tübingen, Germany

Abstract:

In order to test the concept of homology [1, 2] on a lighter pair of nuclei we did focus on the target nuclei ^{90}Zr and ^{91}Zr. To gain the information needed high resolution $(\vec{p},\alpha)$ experiments were carried out. Here we report on the results of the target ^{90}Zr. In the excitation energy range from 0 to approximately 3 MeV 36 levels could be resolved. The data have been analyzed with DWBA-calculations using a double-folded potential in the exit-channel. Moreover the structure of low-lying states of ^{87}Y has been studied within the frame work of shell model, using the code OXBASH.

Experimental setup:

The experiment was carried out at Munich MP Tandem accelerator using a polarized 22 MeV proton beam, the Q3D magnetic spectrograph and the 1.6 m focal plane detector with periodic readout allowing particle identification and focal plane reconstruction [3]. The energy resolution achieved was $\approx$ 12 keV and the uncertainty in the energy attributed to the resolved levels was estimated to be $\pm$ 3 keV. Angular distributions have been measured from 5^o to 65^o in steps of 5^o. The spectrometer entrance slits were adjusted to provide for $\Theta \geq 10^o$ a solid angle of 11.038 msr. The beam current used was about 140 nA with a value for the polarization (both up and down) of (73 $\pm$ 5) %.

A typical spectrum is shown in Fig. 1.

Analysis:

In the analysis of the data finite range DWBA-calculations have been performed. The real part of the α-channel was a double folded optical potential calculated from

$$V(\vec{r}) \;=\; \lambda \cdot \int\int \rho_1(\vec{r}_1)\rho_2(\vec{r}_2)t(E,\rho_1,\rho_2,\vec{r}_1,\vec{r}_2,\vec{r})d\vec{r}_1 d\vec{r}_2.$$

Here $\rho_1(\vec{r}), \rho_2(\vec{r})$ are the respective nucleon densities of target and projectile, $t(E,\rho_1,\rho_2,$ $\vec{r}_1,\vec{r}_2,\vec{r})$ is a parametrisation of the nucleon-nucleon-interaction taken from [4] and λ is a scaling parameter. The nucleon density distributions ρ_1 and ρ_2 were the experimental ones [5] obtained from electron scattering and unfolded with the charge distribution of the proton. For the imaginary part of the optical potential in the exit channel a volume Woods-Saxon-potential was chosen. In a first step the angular distribution and the analyzing power of the g.s. transition were fitted with the code TROMF [6] which allows a simultaneous fit to the elastic data in the entrance and exit channel as well as to the reaction data (Fig. 2). In the entrance channel the potential of Ref. [7] was used. The potential parameters obtained are listed in Table 1. The optical potential in the exit channel agrees well with the results found in a systematic study of the energy and

mass dependence of α-nucleus double-folded potentials [8].

In a second step the cross sections and analyzing powers of all the resolved states found have been computed using the code DWUCK5 [9]. In these calculations only the binding energy of the triton has been adjusted to fit the excitation energy of the level considered. Most of the levels are reproduced quite well (Figs. 3-6).

The advantage of the method applied is that the potential ambiguities on the α-channel are removed through i) the simultaneous fit of both the scattering and the reaction data and ii) the comparison of the potentials obtained with our global α-systematics. This leads to smaller renormalisation factors and a more systematic behaviour of the experimental spectroscopic factors.

Shell model calculations:

The structure of low lying levels of ^{87}Y has been studied in the framework of the shell model. The calculations have been parallely performed for both ^{87}Y and ^{88}Y nuclei, since our interest is concentrated to evidence levels in ^{88}Y homologous to states in ^{87}Y.

Here we present the results for ^{87}Y

The calculation are based on the usual one- and two-body Hamiltonian

$$H = \sum_i \epsilon_i a_i^\dagger a_i + \sum_{ijkl} V_{ijkl} a_i^\dagger a_j^\dagger a_k a_l$$

and we have constructed the model space using the orbitals $1f_{5/2}$, $2p_{3/2}$ and $2p_{1/2}$ for the protons and the orbitals $1g_{9/2}$, $1g_{7/2}$, $2d_{5/2}$, $2d_{3/2}$ and $3s_{1/2}$ for the neutrons. For the two-body matrix elements V_{ijkl} we have used the set GWBXC [12], which are essentially G-matrix effective interactions based on realistic Paris potential.

The calculation has been performed with OXBASH code [13]. The resulting low lying levels and corresponding wave functions for ^{87}Y are listed in Table 2. In this case the model space has been assumed of the form : proton $f_{5/2}[5-6], p_{3/2}[3-4], p_{1/2}[0-2]$ and $g_{9/2}[0-1]$; neutron $g_{9/2}[8]$. In square brackets the allowed particle occupations are indicated.

The single particle energies used in the calculations are:
-8.90 MeV, -12.62 MeV, -9.61 MeV, -5.07 MeV for the $f_{5/2}$, $p_{3/2}$, $p_{1/2}$, $g_{9/2}$ proton orbitals, respectively and 0.664 MeV for the $g_{9/2}$ neutron orbital.

In terms of particle-hole description, $\pi(1h)\nu(1h)$ negative-parity states of the form

$$[\pi(j)^{-1}\nu(g_{9/2})^{-2})_{I_\nu}]_I$$

are used where the allowed proton-hole states include $p_{3/2}$, $f_{5/2}$ and $p_{1/2}$ orbitals, plus $\pi(2h-1p)\nu(2h)$ positive-parity states of the form

$$[\pi[(j_1)^{-1}(j_2)^{-1}(g_{9/2})]_{I_\pi}(\nu(g_{9/2})^{-2})_{I_\nu}]_I,$$

i.e. states corresponding to proton core excitation to the proton $g_{9/2}$ orbital. From the components of the lowest states displayed in the table, one can see that only the spins $1/2^-$ and $9/2^+$ of the lowest states can be assigned to dominant proton single particle configurations $(p_{1/2})^{-1}$ and $(p_{1/2})^{-2}(g_{9/2})$, respectively. In the case of the spins $3/2^-$ and $5/2^-$, the lowest states are still associated, as dominant component, to the proton $(p_{1/2})$ state, with a recoupling of the two $(g_{9/2})$ neutron holes. The states collecting most of the single-hole character are predicted to lie at higher excitation energy, precisely at 1.00 MeV for the $5/2^-$ and 1.46 MeV for the $3/2^-$.

In Tables 3 and 4 all the observed levels of ^{87}Y up to an excitation energy of almost 3 MeV are listed together with those observed in a previous (p,α) experiment [14] and the corresponding adopted ones [15]. From the analysis 10 new attributions of spin and parity values result,improving the present knowledge of the ^{87}Y level scheme.

References

[†] *guest researcher*, permanent address: Soltan Institute for Nuclear Studies, Swierk, Poland.

[‡] *guest researcher*, permanent address: Institute of Modern Physics, Academia Sinica, Lanzhou, P.R.China.

[1] E. Gadioli et al., Phys. Rev. C 43, 2572 (1991)

[2] E. Gadioli *et al.* , Phys. Rev. C 47, 1129 (1993)

[3] E. Zanotti et al., Nucl. Instr. Meth. A 310, 706 (1991)

[4] A. M. Kobos *et al.* , Nucl. Phys. A384, 65 (1982)

[5] H. de Vries et al., Nucl. Data Tables 36, 495 (1987)

[6] M. Walz, code TROMF, University of Tübingen, 1987, unpublished

[7] R. L. Varner *at al.* , Phys. Rep. 201, 57 (1991)

[8] H. Abele, Ph.D. thesis , University of Tübingen, 1992

[9] P. D. Kunz, code DWUCK5, University of Colorado, unpublished

[10] J. B. England et al., Nucl. Phys. A388, 573 (1982)

[11] J. B. Ball et al., Phys. Rev. 135, B706 (1964)

[12] A. Hosaka et al., Nucl. Phys. A444, 76 (1985)

[13] A. Etchegoyen et al., MSU-NSCL Report 524, (1985)

[14] R. J. Peterson, and H. Rudoph, Nucl. Phys. A241, 253 (1975)

[15] H. Sievers, Nuclear Data Sheets 62, 327 (1991)

	V_r	r_r	a_r	W	r_w	a_w
p	52.4	1.20	0.690	1.12	1.236	0.690
α	$\lambda = 1.204$			8.33	1.83	0.576
t		1.24	1.19			
	W_d	r_d	a_d	V_{so}	r_{so}	a_{so}
p	8.27	1.236	0.690	5.90	1.072	0.630

TABLE 1: Table with the potential parameter used in the calculations

E(MeV)		J^π	j				CONFIGURATION
Exp.	Th.		$p_{1/2}$	$p_{3/2}$	$f_{5/2}$		
0.000	0.000	$1/2^-$	87.05	5.14	7.81		$[\pi(j)^{-1}\nu(g_{9/2})^2_{I\nu}]_I$
0.794	0.691	$5/2^-$	57.39	3.01	39.59		$[\pi(j)^{-1}\nu(g_{9/2})^2_{I\nu}]_I$
0.982	0.689	$3/2^-$	77.68	17.70	4.62		$[\pi(j)^{-1}\nu(g_{9/2})^2_{I\nu}]_I$
1.184	1.464	$3/2^-$	10.87	78.21	10.92		$[\pi(j)^{-1}\nu(g_{9/2})^2_{I\nu}]_I$
1.201	1.000	$5/2^-$	26.65	3.61	69.74		$[\pi(j)^{-1}\nu(g_{9/2})^2_{I\nu}]_I$
			j_1j_2				
			$p_{1/2}(2)$	$p_{1/2}p_{3/2}$	$f_{5/2}p_{1/2}$	$f_{5/2}p_{3/2}$	
0.382	0.379	$9/2^+$	77.16	7.14	14.61	1.09	$[\pi[(j_1)^{-1}(j_2)^{-1}(g_{9/2})]_{I\pi}$ $[\nu(g_{9/2})^2]_{I\nu}]_I$

TABLE 2: Eigenvalues and percentage of different components obtained within the Shell Model Hamiltonian with GWBXC interaction for low lying states of ^{87}Y

Present work		*(p, α) reaction* [14]		*Adopted levels* [15]	
E_x	J^π	E_x	J^π	E_x	J^π
0	$\frac{1}{2}^-$	0	$\frac{1}{2}^-$	0	$\frac{1}{2}^-$
0.379	$\frac{9}{2}^+$	0.38	$\frac{9}{2}^+$	0.381	$\frac{9}{2}^+$
0.793	$\frac{5}{2}^-$	0.79	$\frac{5}{2}^-$	0.794	$\frac{5}{2}^-$
0.981	$\frac{3}{2}^-$	0.99	$\frac{3}{2}^-$	0.981	$\frac{3}{2}^-$
1.151	$\frac{5}{2}^+$	1.15	$(\frac{3}{2}^-)$	1.153	$(\frac{5}{2})^+$
1.182	$\frac{3}{2}^-$			1.178	$(\frac{3}{2})^-$
1.201	$\frac{5}{2}^-$	1.20	$(\frac{5}{2}^-)$	1.202	$(\frac{5}{2})^-$
		1.37			
1.401	$(\frac{13}{2}^+)$			1.404	$(\frac{13}{2}^+)$
		1.58			
1.607	$(\frac{5}{2}^+)$			1.609	$\frac{3}{2}^-, \frac{5}{2}^-$
1.629	$\frac{5}{2}^+$			1.623	$(\frac{5}{2}, \frac{7}{2})$
1.704	$\frac{3}{2}^-$			1.704	$(\frac{5}{2}^-)$
1.757	$\frac{5}{2}^+$			1.757	$(\frac{5}{2}^+, \frac{7}{2}^-)$
		1.79	$\frac{5}{2}^-$		
1.802	$\frac{5}{2}^-$			1.801	$(\frac{1}{2}^-, \frac{3}{2}, \frac{5}{2}^-)$
1.846	$\frac{1}{2}^-$	1.85	$\frac{3}{2}^-$	1.851	$\frac{1}{2}^-$
1.979	$\frac{7}{2}^-$			1.988	$(\frac{7}{2}, \frac{9}{2})^-$
2.006	$\frac{11}{2}^+$			2.008	$(\frac{7}{2})$
2.113	$\frac{5}{2}^+$			2.111	
		2.13	$(\frac{7}{2}^-)$		
2.153	$\frac{9}{2}^-$			2.159	
2.184	$\frac{7}{2}^-$			2.185	
2.209	$\frac{3}{2}^-$			2.207	$(\frac{15}{2}^+, \frac{17}{2}^+)$
				2.210	$\frac{1}{2}$

TABLE 3: Found levels

Present work		*(p,α) reaction [14]*		*Adopted levels [15]*	
E_x	J^π	E_x	J^π	E_x	J^π
				2.242	$(\frac{7}{2},\frac{9}{2}^-)$
2.249	$\frac{9}{2}^-$			2.244	
				2.274	$(\frac{9}{2}^+)$
2.276	$\frac{9}{2}^-$			2.278	$(\frac{7}{2}^-)$
2.302	$\frac{11}{2}^-$	2.30	$(\frac{9}{2}^+)$		
				2.354	
2.365	$(\frac{15}{2}^- + \frac{7}{2}^+)$			2.367	$(\frac{15}{2}^-)$
2.408	$\frac{3}{2}^-$			2.409	$(\frac{3}{2})^+$
2.449	$\frac{9}{2}^-$			2.446	$(\frac{5}{2})^+$
2.531	$\frac{11}{2}^-$			2.532	
2.562	$\frac{11}{2}^+$	2.57	$(\frac{15}{2}^-)$	2.564	$(\frac{9}{2})^+$
				2.572	$(\frac{3}{2}^-)$
2.599	$\frac{9}{2}^-$			2.595	
		2.63	$(\frac{13}{2}^-)$		
2.661	$\frac{7}{2}^+$				
2.682	$\frac{11}{2}^-$			2.676	$(\frac{17}{2})^-$
2.747	$\frac{3}{2}^+$				
2.801	$\frac{11}{2}^+$				
				2.827	$(\frac{21}{2})^+$
				2.828	$(\frac{3}{2}^-,\frac{5}{2}^-)$
2.831	$\frac{9}{2}^-$				
2.903	$\frac{3}{2}^-$			2.901	$\frac{3}{2}^-,\frac{5}{2}^-$
		2.96	$\frac{5}{2}^+$		
2.998	$\frac{5}{2}^+$			2.995	$(\frac{5}{2})^+$

TABLE 4: Found levels

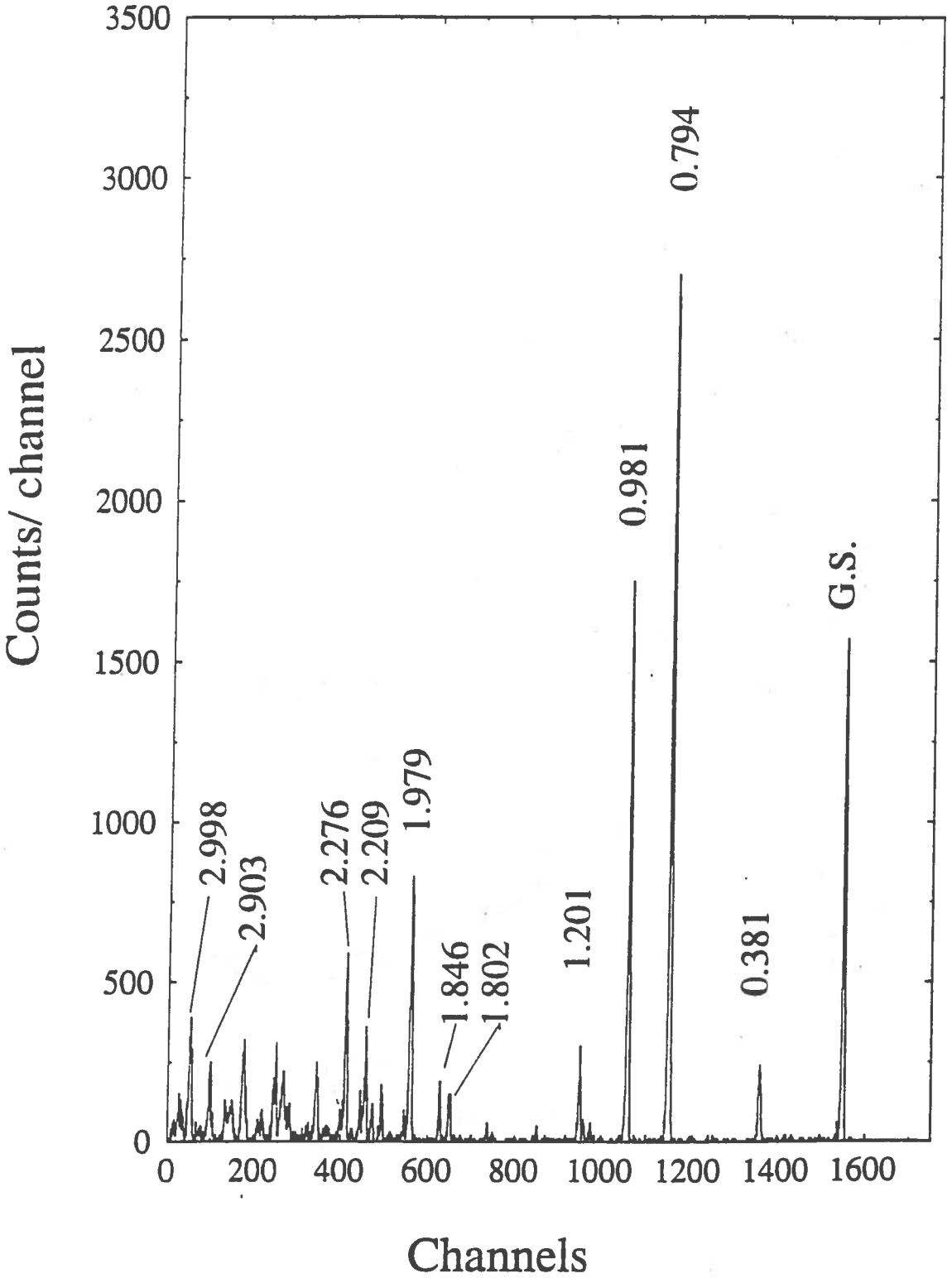

FIGURE 1: Typical spectrum obtained in the experiment at $\theta_{lab} = 20^{o}$. For some of the levels the excitation energy is indicated.

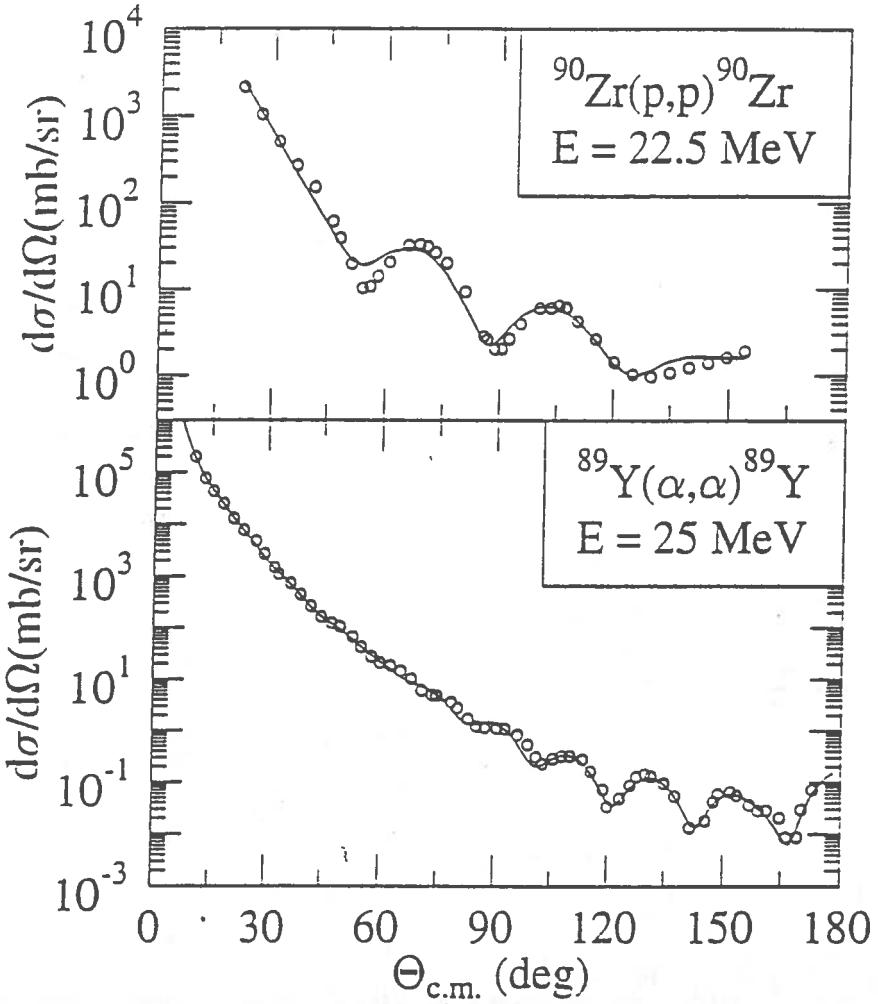

FIGURE 2: Differential cross sections in the entrance and exit channel. The experimental data are taken from [10] and [11]. The solid lines are optical model calculations with the potential parameters listed in table 1.

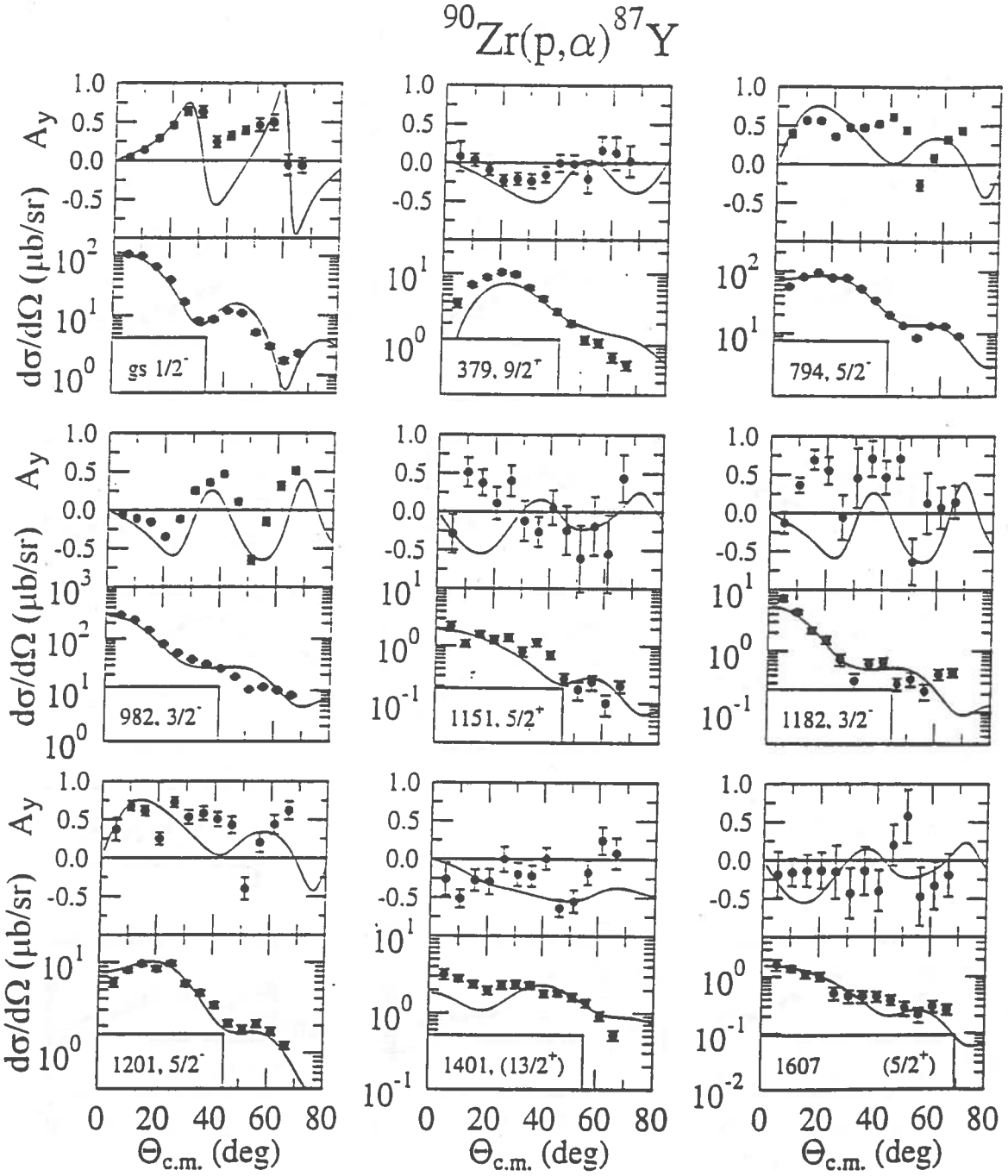

FIGURE 3: Differential cross sections and asymmetries for the $(\vec{p},\alpha)$ reaction.

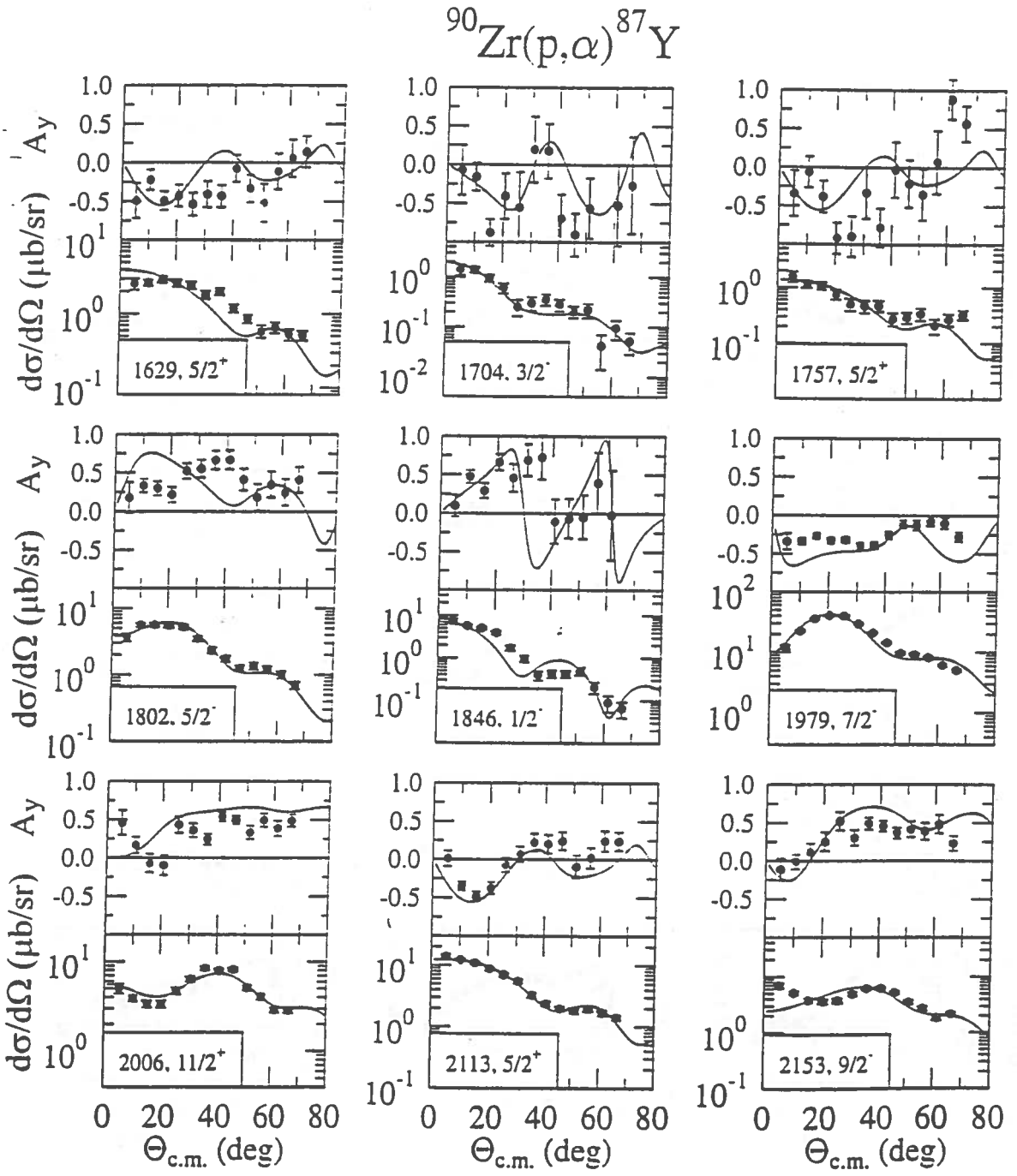

FIGURE 4: Differential cross sections and asymmetries for the $(\vec{p}, \alpha)$ reaction.

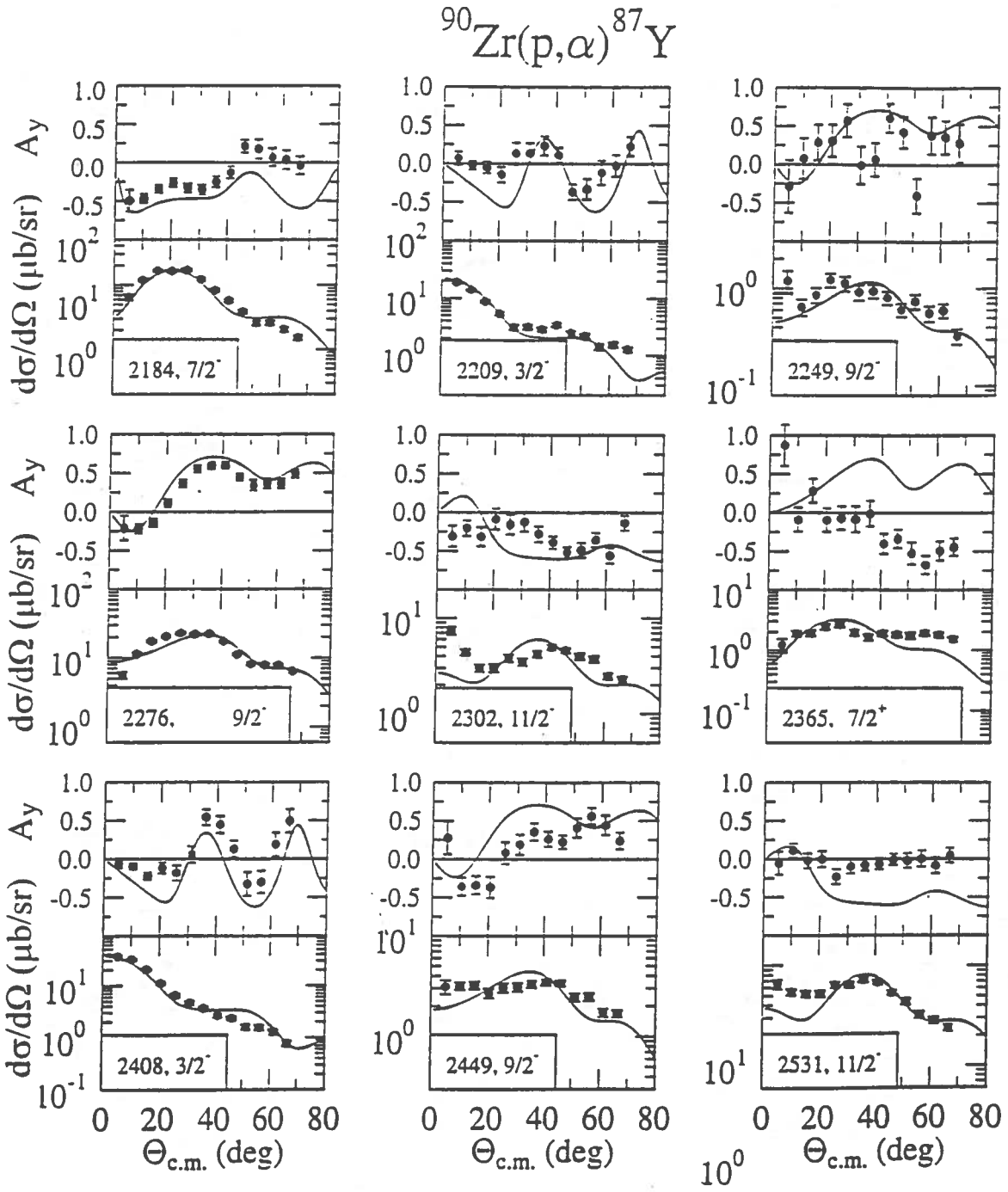

FIGURE 5: Differential cross sections and asymmetries for the $(\vec{p},\alpha)$ reaction.

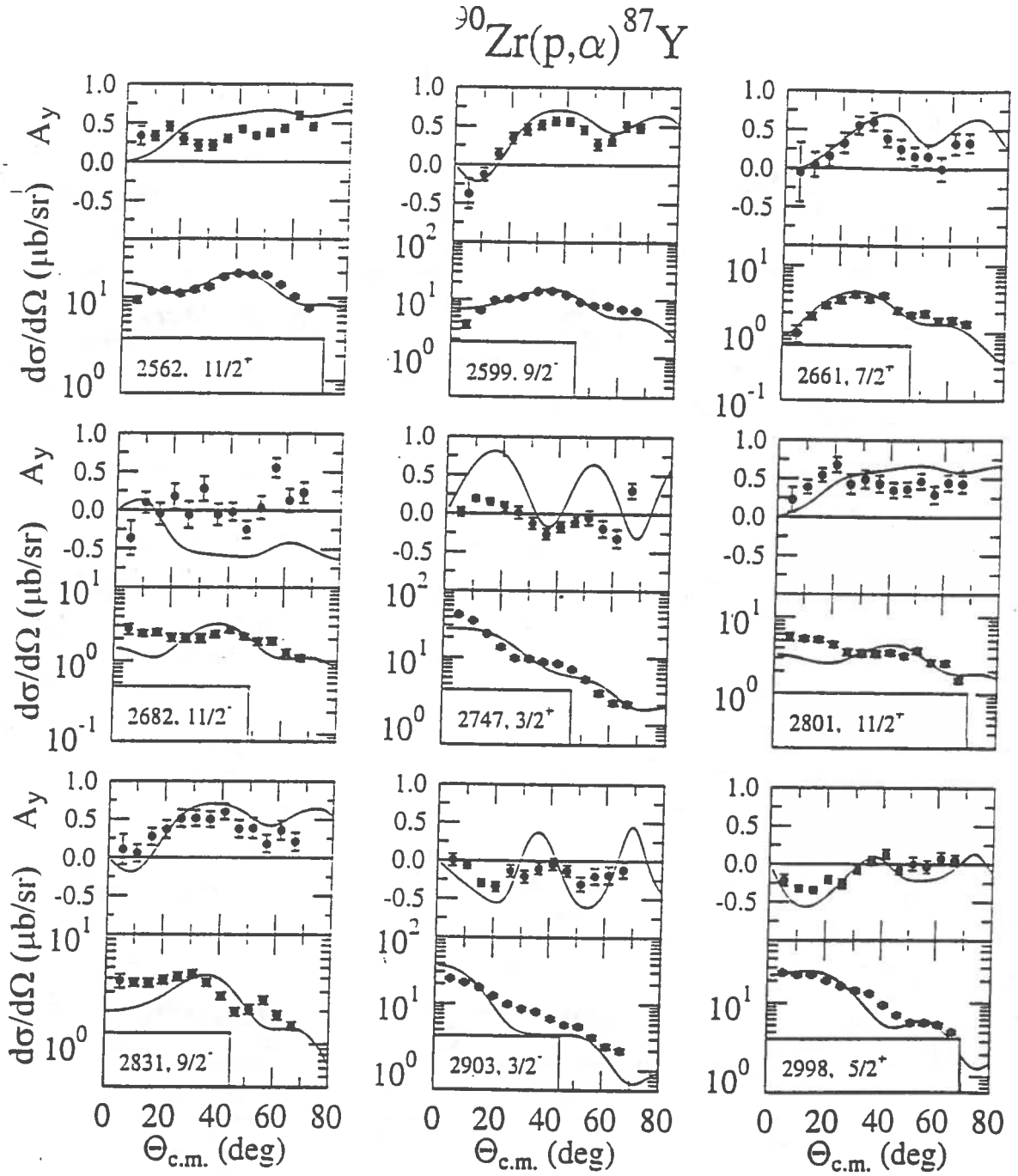

FIGURE 6: Differential cross sections and asymmetries for the $(\vec{p},\alpha)$ reaction.